Supplementary Information (SI) for Journal of Materials Chemistry A.
This journal is © The Royal Society of Chemistry 2025

Desired spontaneous corrosion via a highly hydrophilic porous layer for aqueous zinc-ion batteries

Guoquan Jiang [a], Junchao Zhu [a], Linxin He [a], Nan Qiu [a] and Yuan Wang [a]**

[a] Key Laboratory of Radiation Physics and Technology of Ministry of Education, Institute of Nuclear Science and Technology, Sichuan University, Chengdu 610064, P. R. China

** Corresponding authors.*

E-mail addresses: qiun@scu.edu.cn; wyuan@scu.edu.cn

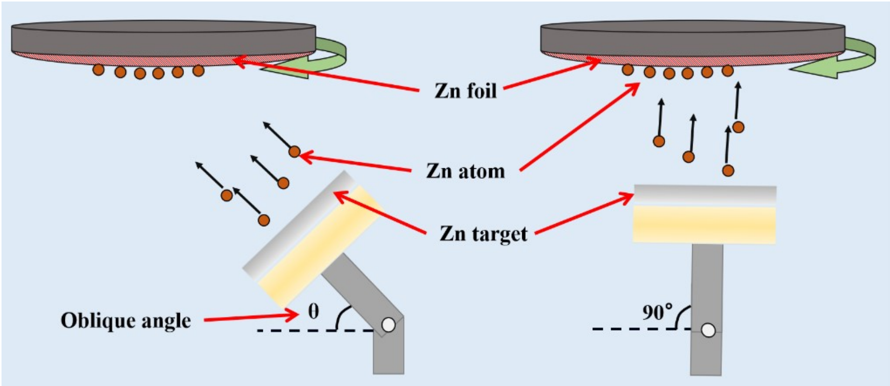

Fig. S1. Schematic diagram of oblique angle (30°, 45° and 60°) and vertical sputtering (90°) in a magnetron sputtering chamber.

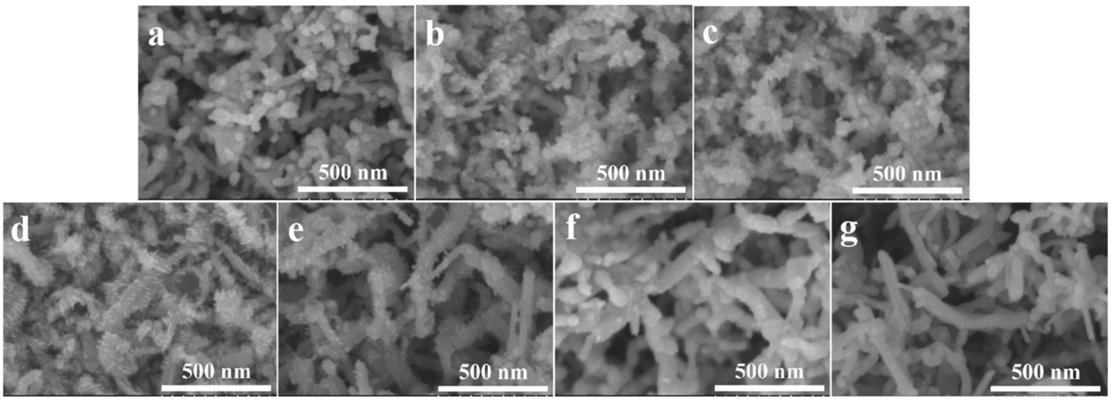

Fig. S2. (a-g) SEM images of Zn-30, Zn-45, Zn-60, Zn-2, Zn-5, Zn-8, and Zn-15, respectively, at a scale of 500 nm.

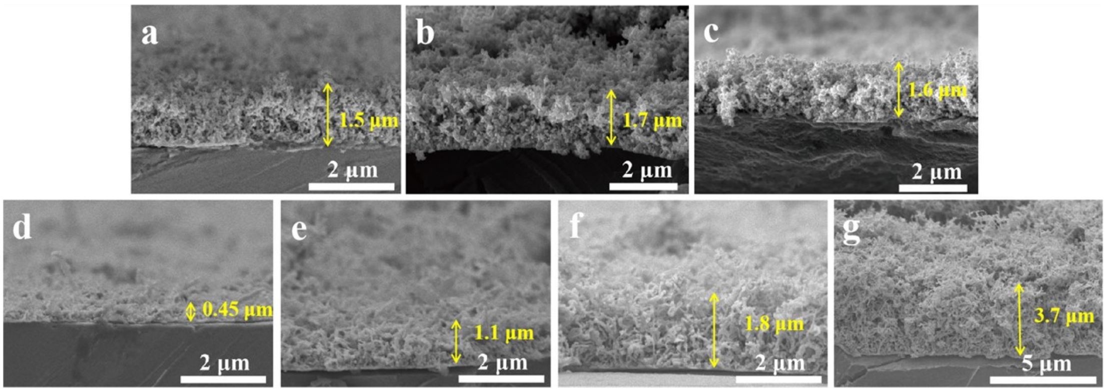

Fig. S3. (a-g) Cross-sectional SEM images of Zn-30, Zn-45, Zn-60, Zn-2, Zn-5, Zn-8 and Zn-15, respectively.

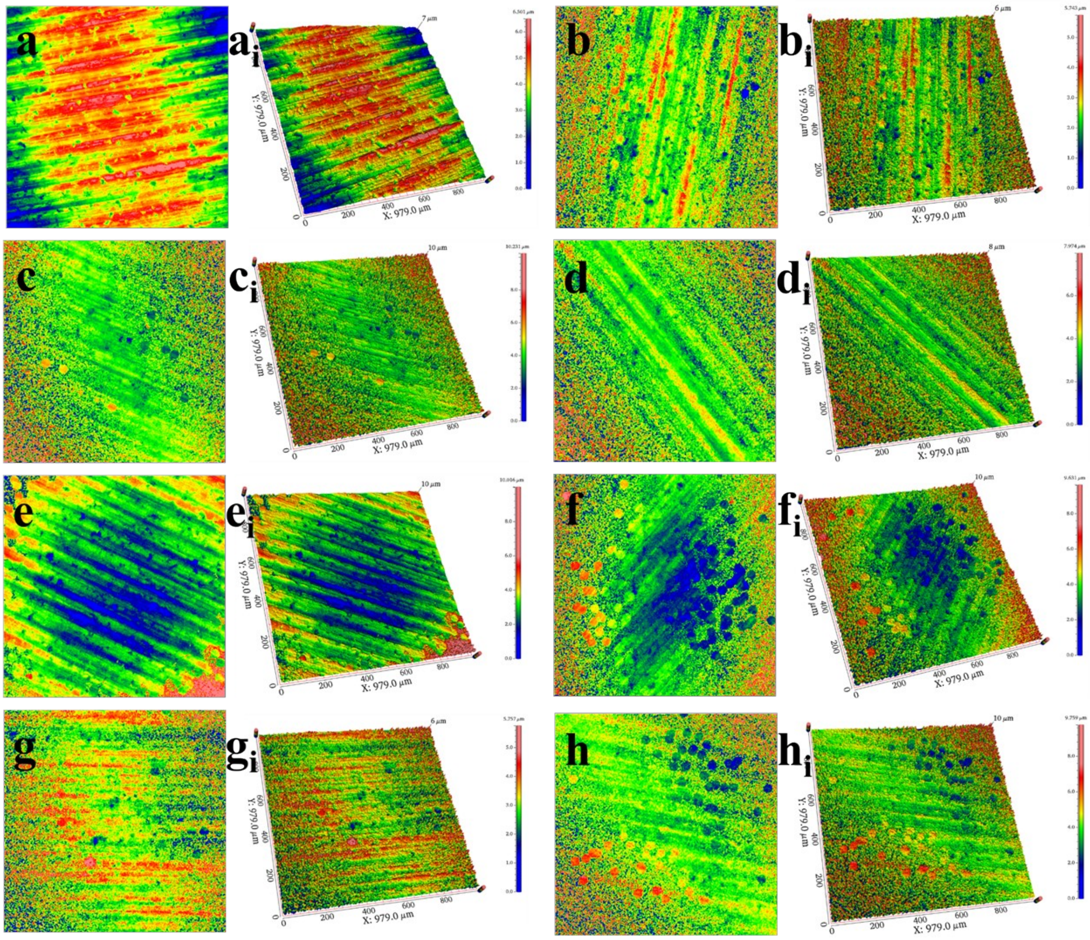

Fig. S4. (a-h) 2D and 3D views of bare-Zn, Zn-30, Zn-45, Zn-60, Zn-2, Zn-5, Zn-8 and Zn-15, respectively.

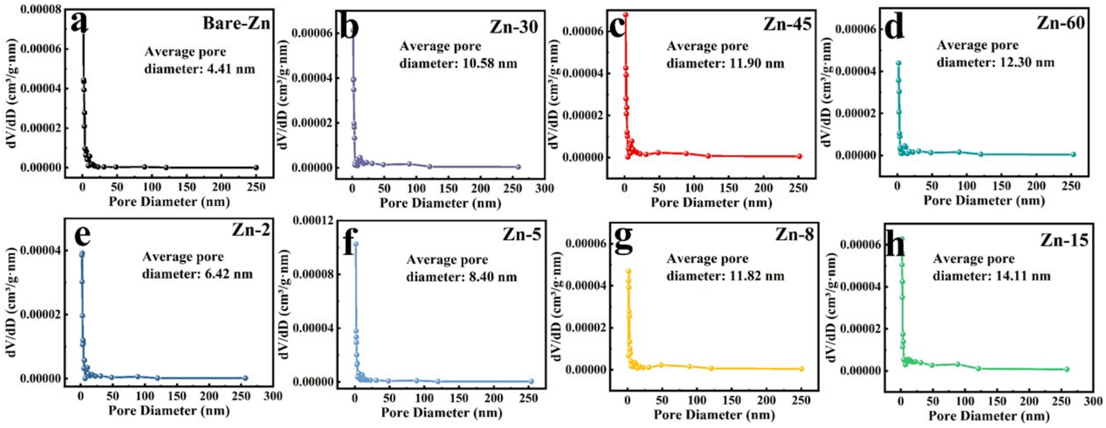

Fig. S5. (a-h) Pore size distribution curves of bare-Zn, Zn-30, Zn-45, Zn-60, Zn-2, Zn-5, Zn-8 and Zn-15, respectively.

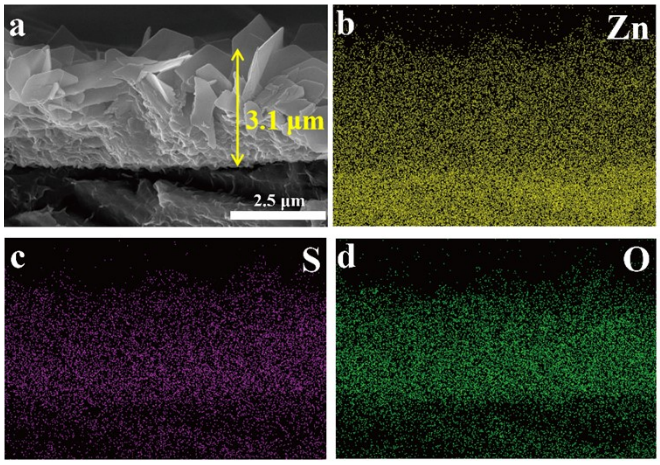

Fig. S6. (a) Cross-sectional SEM image of Zn-45 and (b-d) the corresponding EDX mapping images of Zn, S, and O, respectively.

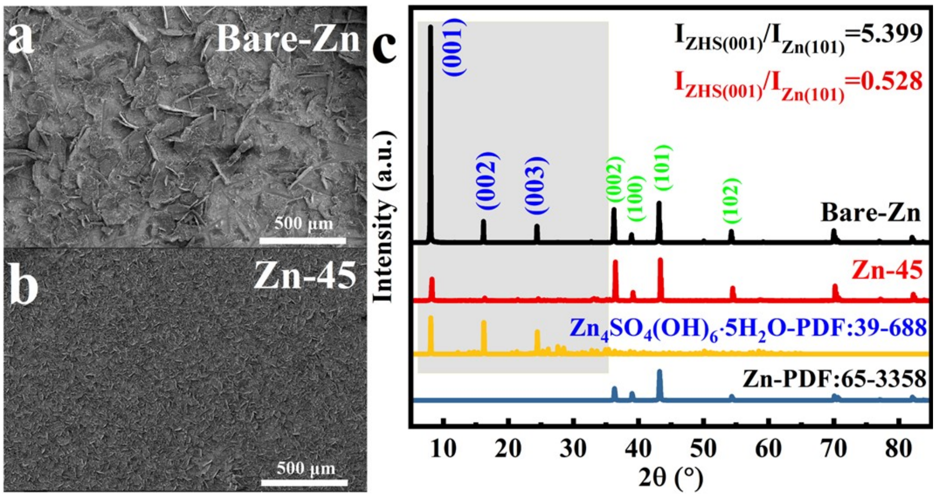

Fig. S7. (a and b) SEM images of bare-Zn and Zn-45 after 7 days of resting, respectively; (c) XRD patterns of bare-Zn and Zn-45 after 7 days of resting.

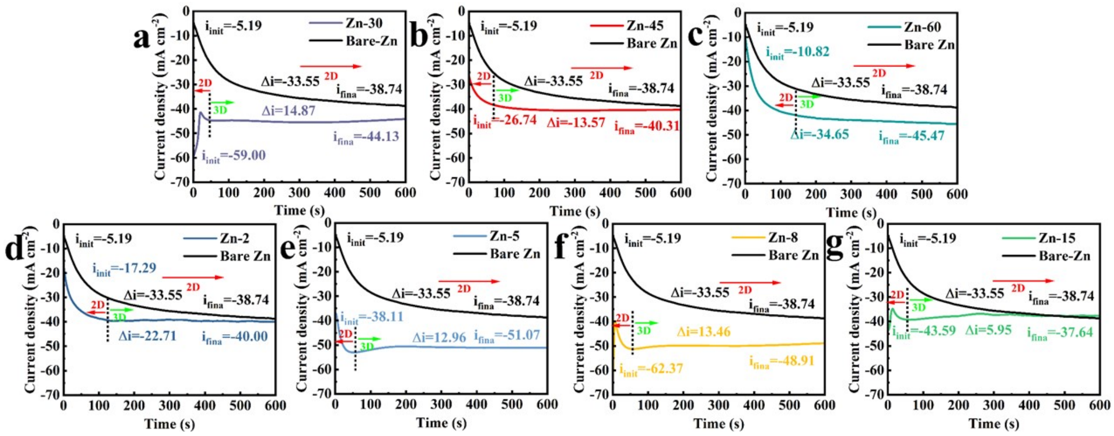

Fig. S8. (a-g) Chronoamperograms (CAs) of bare-Zn, Zn-30, Zn-45, Zn-60, Zn-2, Zn-5, Zn-8 and Zn-15 at an overpotential of -150 mV, respectively.

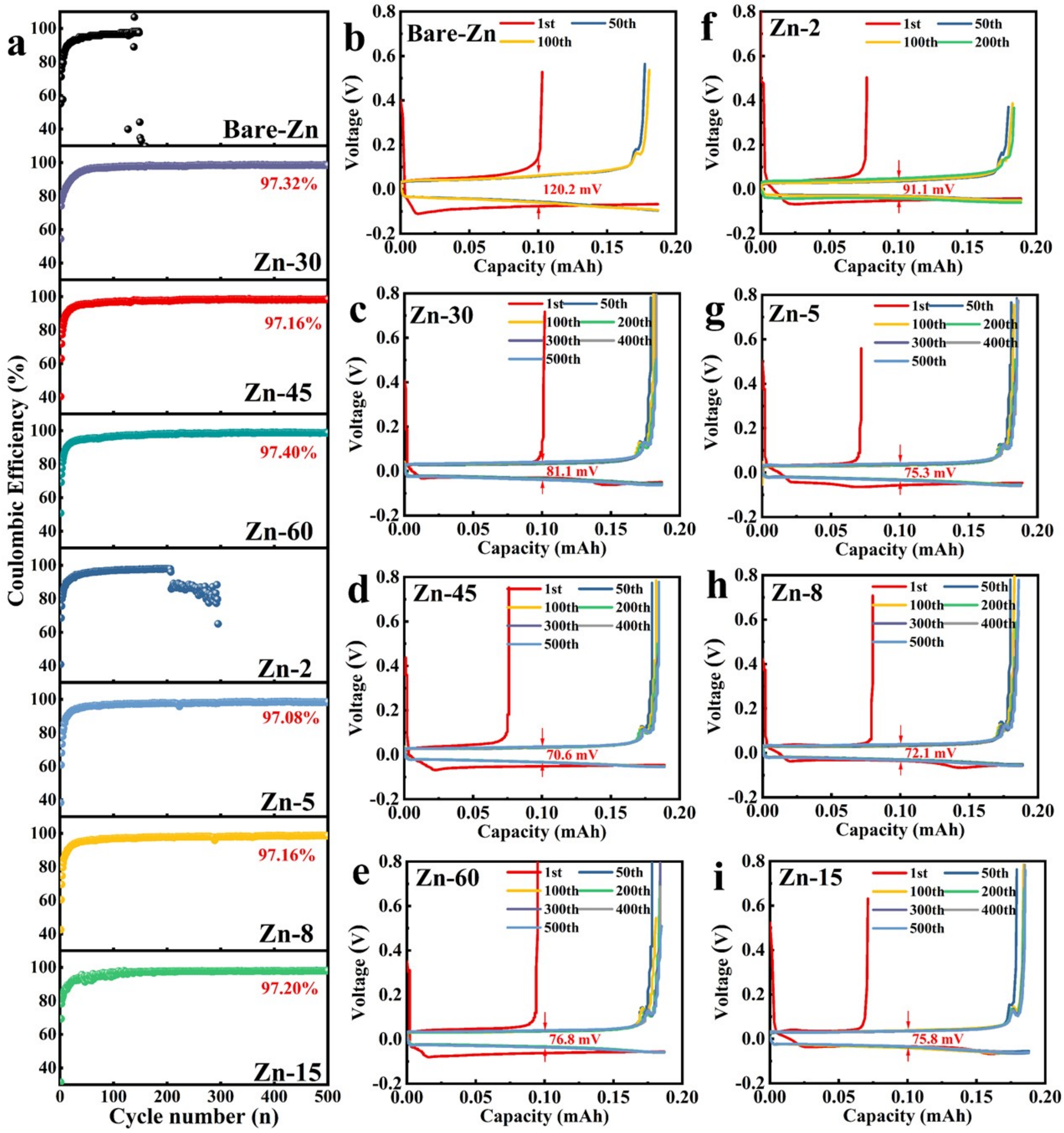

Fig. S9. (a) Coulombic efficiencies of bare-Zn, Zn-30, Zn-45, Zn-60, Zn-2, Zn-5, Zn-8 and Zn-15 asymmetric batteries at 1 mA cm^{-2}; (b-i) Voltage profiles of bare-Zn, Zn-30, Zn-45, Zn-60, Zn-2, Zn-5, Zn-8 and Zn-15 asymmetric batteries at different cycles, respectively.

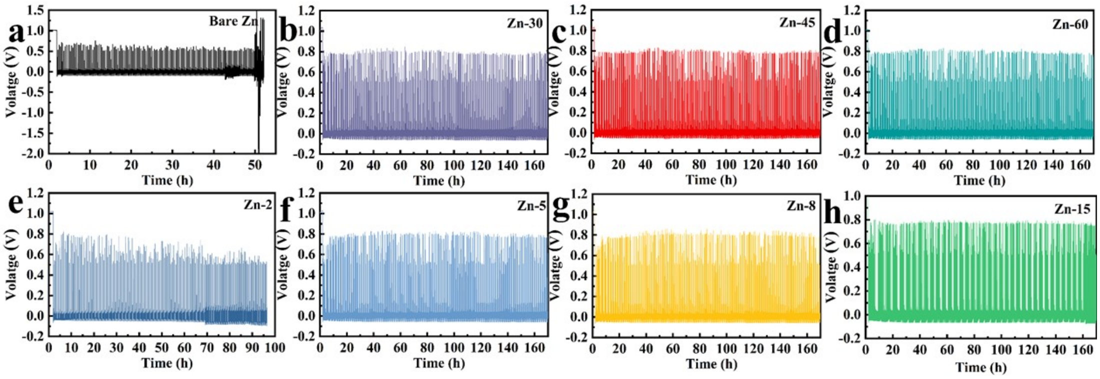

Fig. S10. (a-h) Voltage-time curves of bare-Zn, Zn-30, Zn-45, Zn-60, Zn-2, Zn-5, Zn-8 and Zn-15 asymmetric batteries, respectively.

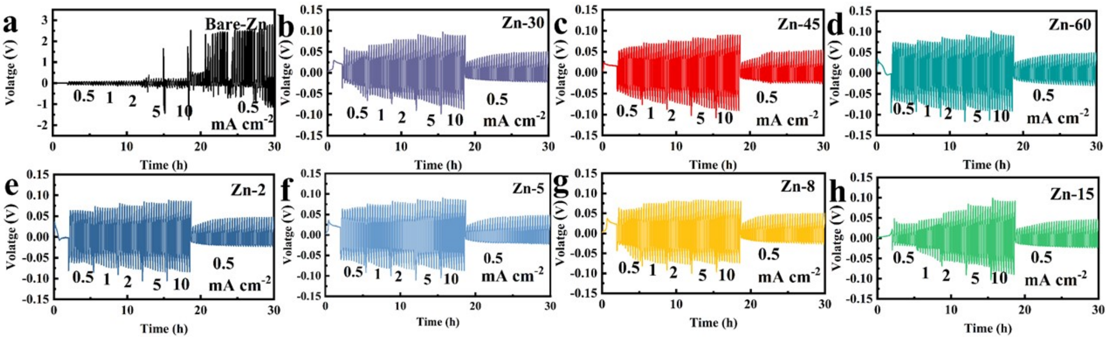

Fig. S11. (a-h) Rate performance of bare-Zn, Zn-30, Zn-45, Zn-60, Zn-2, Zn-5, Zn-8, and Zn-15 symmetric batteries, respectively, at different current densities (0.5, 1, 2, 5, and 10 mA cm^{-2}).

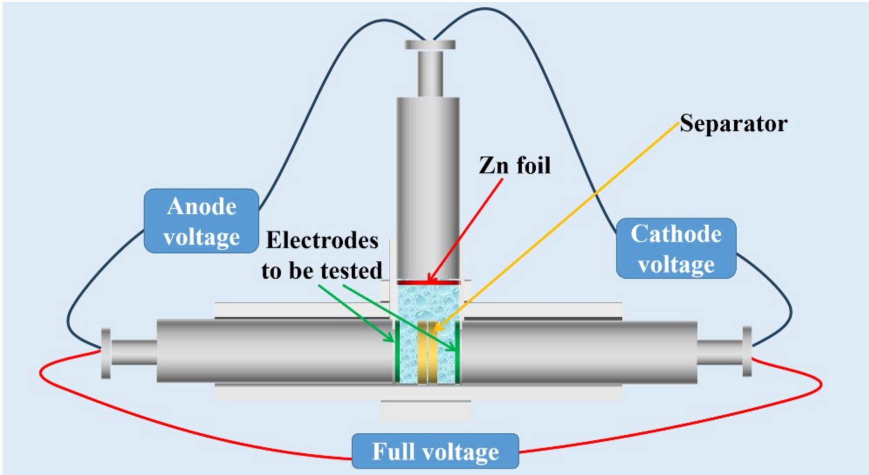

Fig. S12. Schematic diagram of the three-electrode device. The device contains two electrodes to be tested (bare-Zn/sputtering-Zn) and the reference electrode was untreated Zn foil.

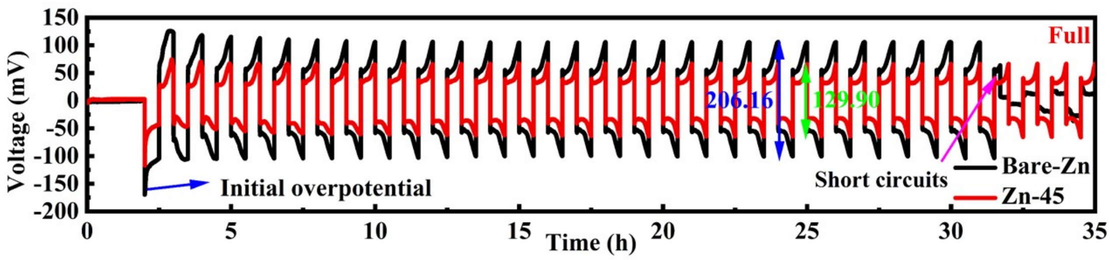

Fig. S13. Voltage-time curves of bare-Zn and Zn-45 of the full tests at 2 mA cm^{-2} with 1 mAh cm^{-2}.

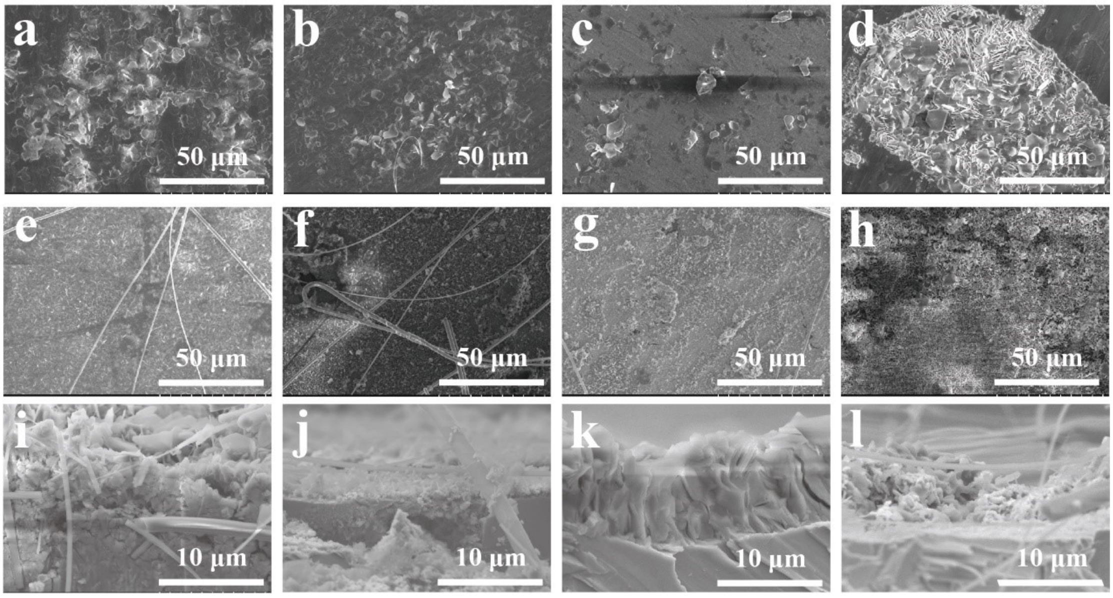

Fig. S14. (a-d) SEM images of bare-Zn under different cycles (10th, 20th, and 30th), respectively; (e-h) SEM images of Zn-45 under different cycles (10th, 20th, and 30th), respectively; (i-l) Cross-sectional SEM images of Zn-45 after different cycles (10th, 20th and 30th), respectively.

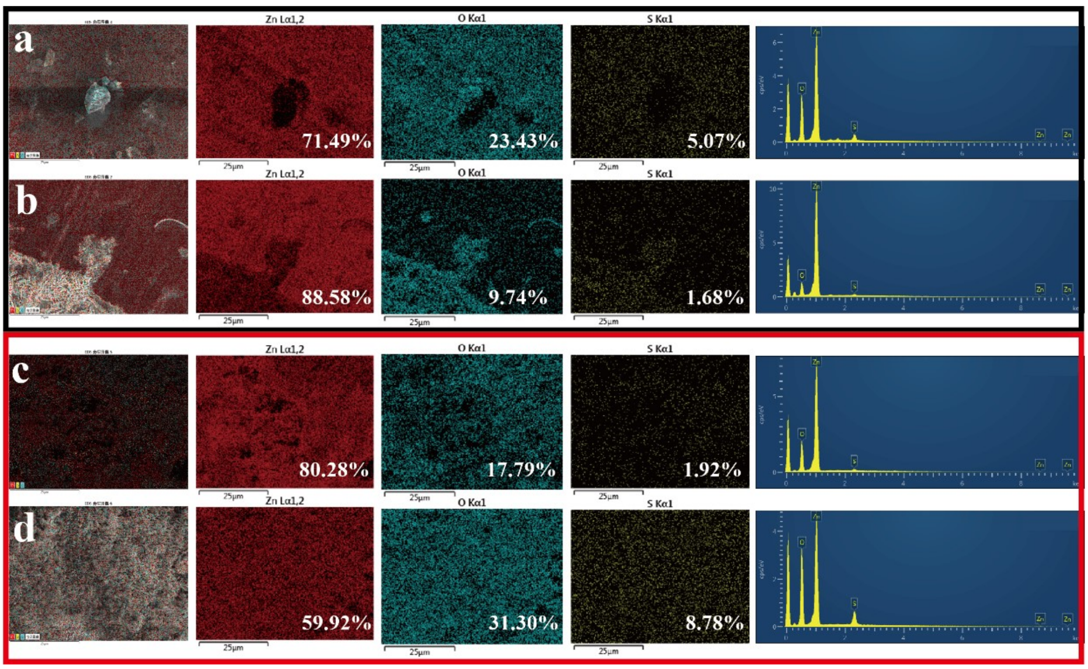

Fig. S15. (a-d) EDX mapping images of bare-Zn and Zn-45 after different cycles (20th and 30th), respectively.

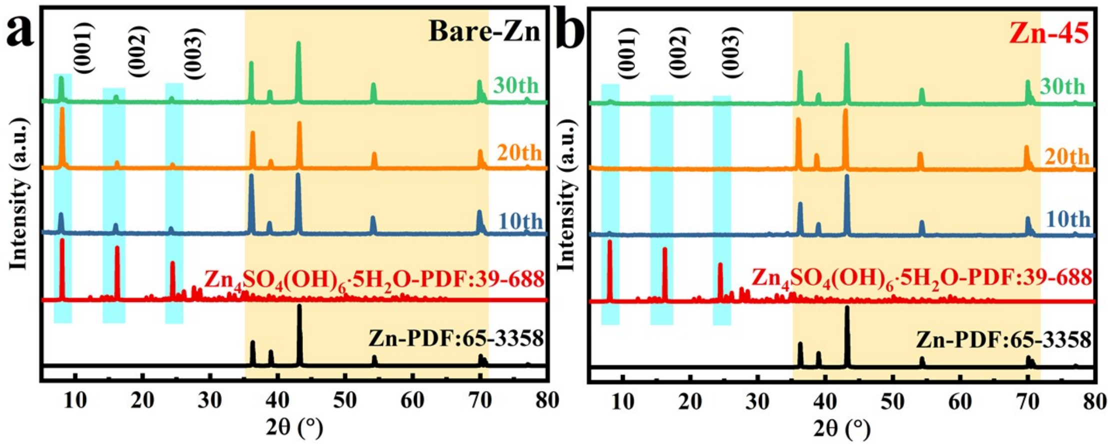

Fig. S16. (a and b) XRD patterns of bare-Zn and Zn-45 after different cycles (10th, 20th, and 30th), respectively.

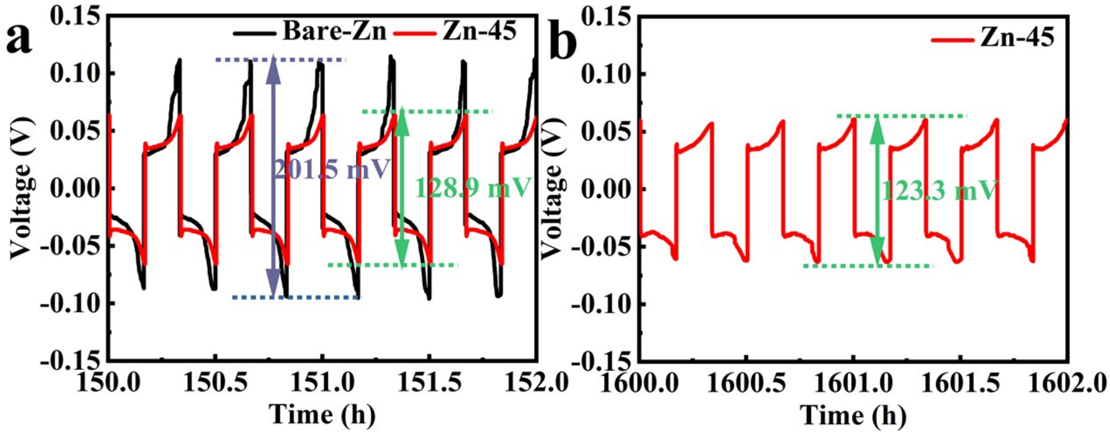

Fig. S17. (a and b) Voltage-time curves of bare-Zn and Zn-45 symmetric batteries at 1 mA cm^{-2} in 150-152 h and 1600-1602 h, respectively.

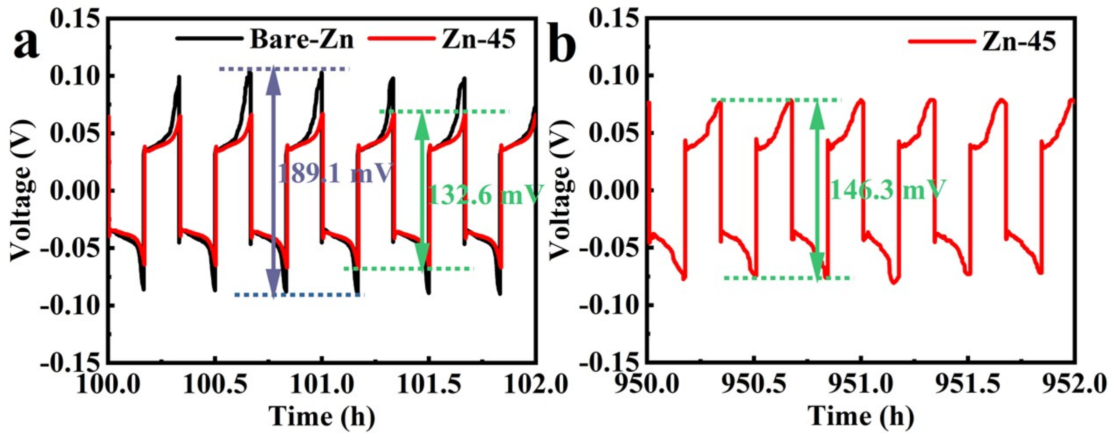

Fig. S18. (a and b) Voltage-time curves of bare-Zn and Zn-45 symmetric batteries at 2 mA cm^{-2} in 100-102 h and 950-952 h, respectively.

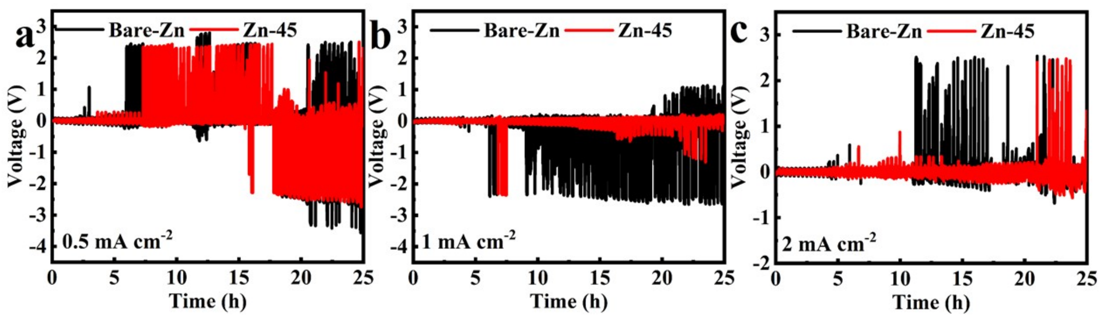

Fig. S19. (a-c) Under no resting time conditions, voltage-time curves of bare-Zn and Zn-45 symmetric batteries at 0.5, 1 and 2 mA cm^{-2}, respectively.

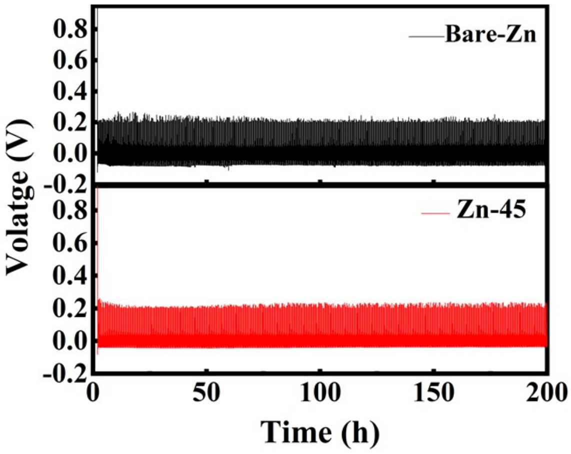

Fig. S20. Voltage-time curves of bare-Zn and Zn-45 asymmetric batteries at 2 mA cm^{-2}.

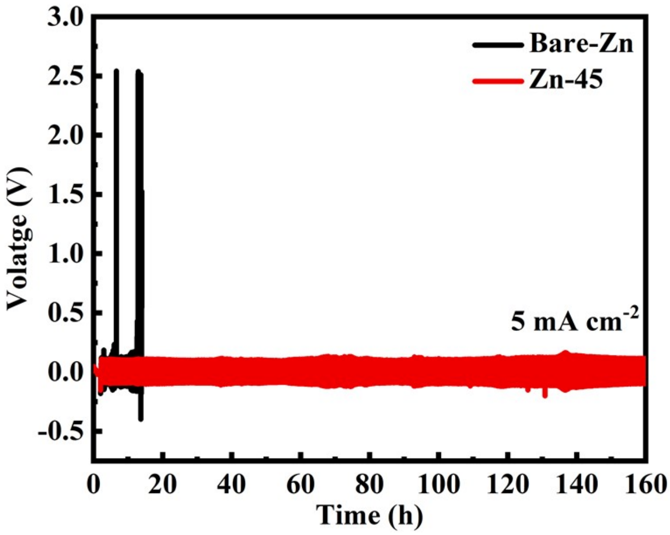

Fig. S21. Long-team cycling performance of bare-Zn and Zn-45 symmetric batteries at 5 mA cm^{-2}.

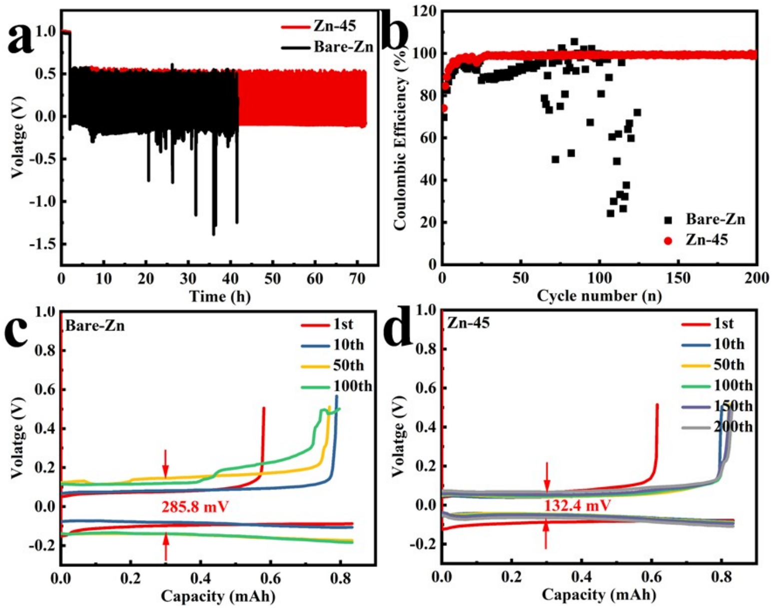

Fig. S22. (a) Voltage-time curves of bare-Zn and Zn-45 asymmetric batteries at 5 mA cm^{-2}; (b) Coulombic efficiency of bare-Zn and Zn-45 asymmetric batteries at 5 mA cm^{-2}; (c and d) Voltage-capacity curves of bare-Zn and Zn-45 at 5 mA cm^{-2}, respectively.

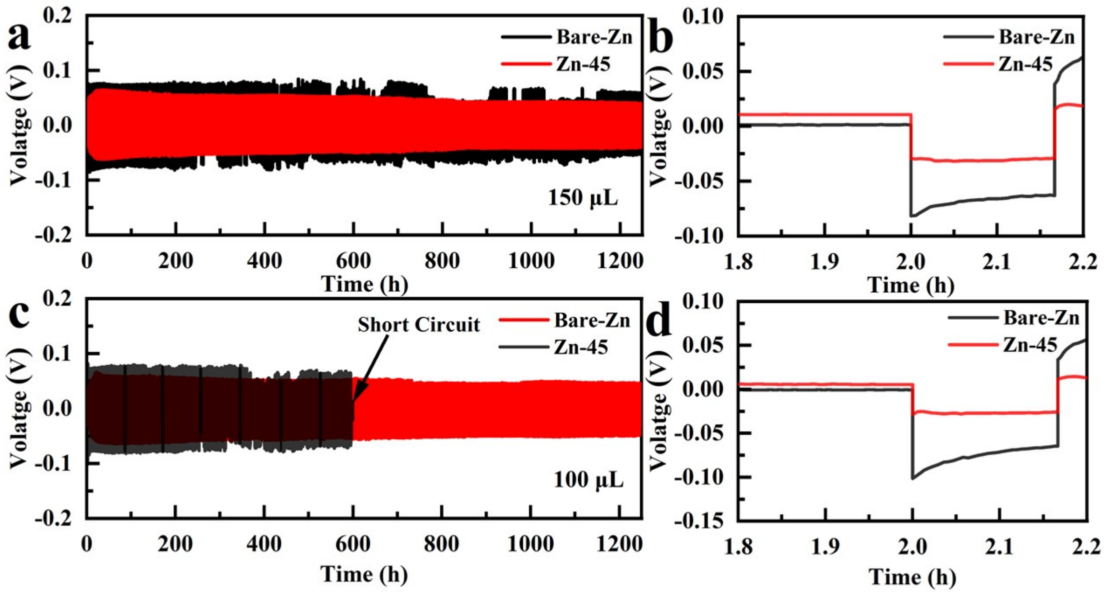

Fig. S23. (a and c) The cycling stability test and (b and d) the corresponding initial discharge curve of the Zn-45 and bare-Zn symmetric batteries with the amount of electrolyte is 150 μL and 100 μL at 0.5 mA cm^{-2}, respectively.

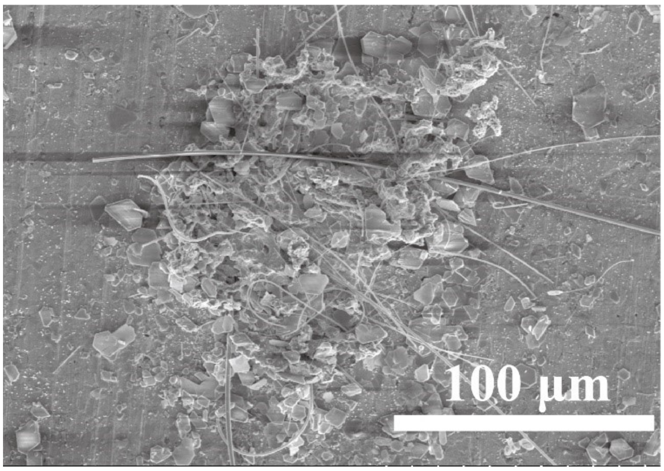

Fig. S24. SEM images of bare-Zn after 550 cycles at a size of 100 μm.

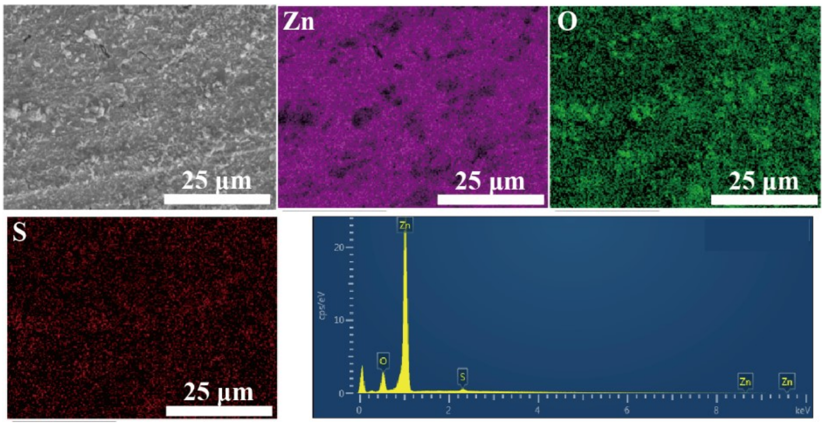

Fig. S25. EDX images of Zn-45 after 550 cycles.

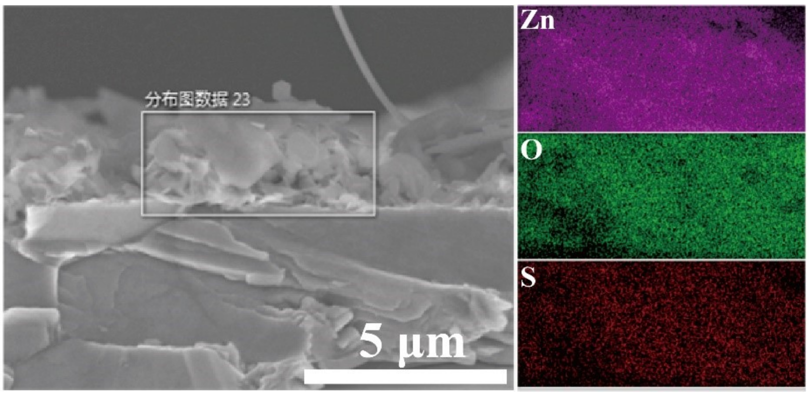

Fig. S26. Cross-sectional EDX images of Zn-45 after 550 cycles.

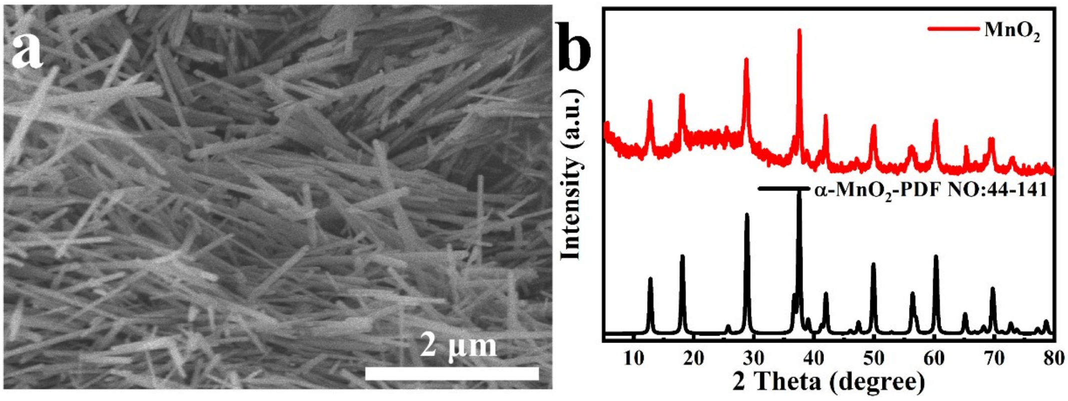

Fig. S27. (a) SEM image of α-MnO_2; (b) XRD pattern of α-MnO_2.

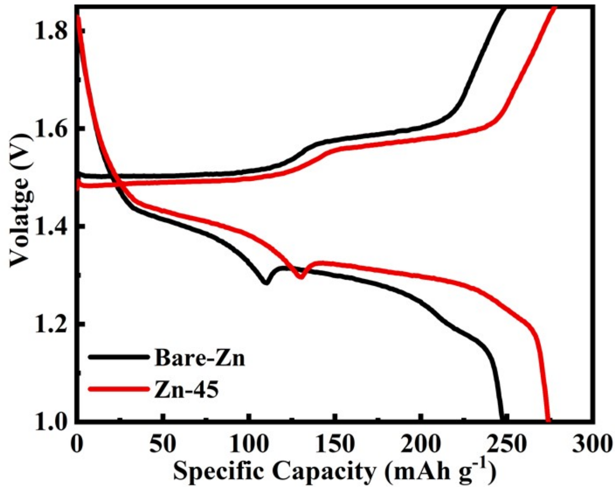

Fig. S28. Galvanostatic charge-discharge curves of bare-Zn and Zn-45 full batteries at 0.2 A g^{-1}.

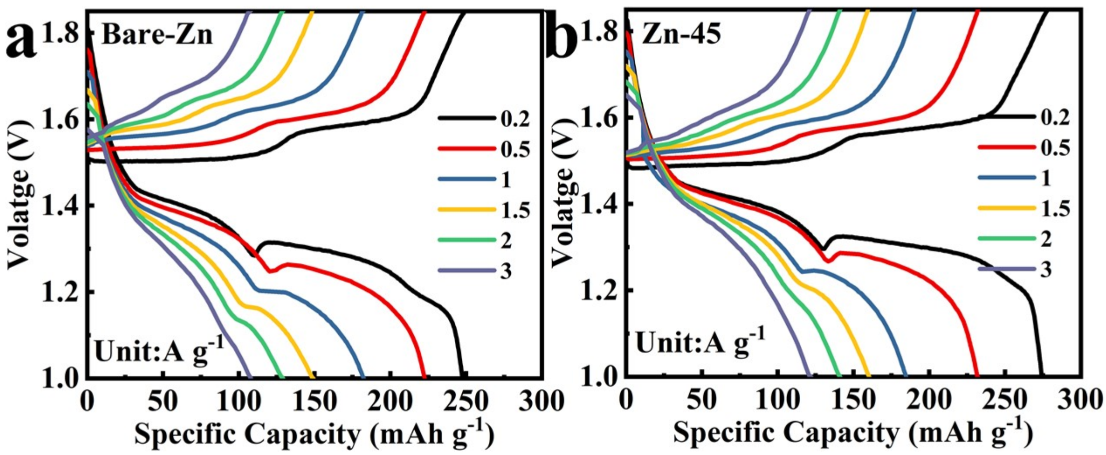

Fig. S29. (a and b) Galvanostatic charge-discharge curves of bare-Zn and Zn-45 full batteries at different current densities, respectively.

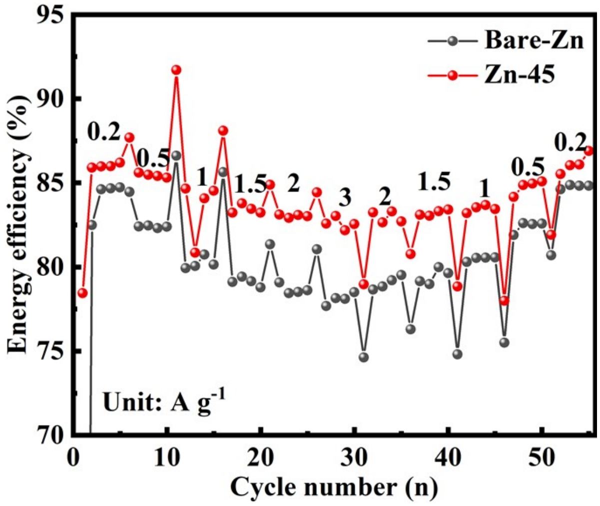

Fig. S30. Energy efficiency of bare-Zn and Zn-45 full batteries at different current densities.

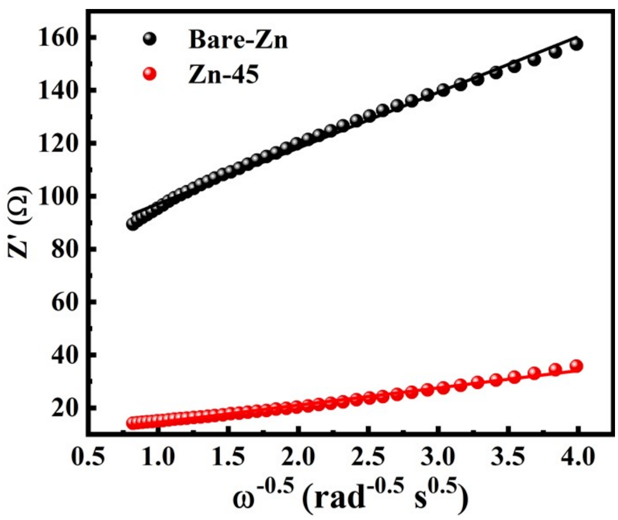

Fig. S31. Corresponding real parts of the impedance (Z') versus reciprocal square root of the angular frequencies (ω) in the low-frequency region.

The ion-diffusion coefficient (D) was obtained from the low-frequency region using the equation (1):[1]

$$D = \frac{R^2T^2}{2A^2n^4F^4C^2\sigma^2} \tag{1}$$

In this equation, R represents the gas constant, T is the absolute temperature, A

denotes electrode area, n indicates the number of transferred electrons, F corresponds to the Faraday constant, C refers to the concentration of Zn^{2+} ions in the electrolyte, and σ stands for the Warburg coefficient. The σ value was determined from the slope of the Z' vs. $\omega^{-0.5}$ plot (Fig. S31), based on the relationship Z' = Rs + Rct + $\sigma\omega^{-0.5}$. The calculated ion-diffusion coefficient for the Zn-45 full batteries was ~5.1×10^{-11} cm^2 s^{-1}, which is significantly higher than for the bare-Zn electrode (~4.8×10^{-12} cm^2 s^{-1}). The reduction in the σ value of the Zn-45 electrode implies an augmentation in ionic conductivity. This is attributed to the composite layer of ZHS and porous zinc, which facilitates the rapid stripping and plating of zinc ions, thereby enhancing the performance of the full battery.

Table S1. Surface roughness parameters of the bare-Zn, Zn-30, Zn-45, Zn-60, Zn-2, Zn-5, Zn-8 and Zn-15, respectively.

Parameter	Bare-Zn	Zn-30	Zn-45	Zn-60	90°			
					Zn-2	Zn-5	Zn-8	Zn-15
Ra (nm)	774.17	571.17	1249.43	774.45	699.27	1075.99	562.90	873.63

Table S2 The typical parameters and cycling performance of Zn-45° compared with some reported Zn-based symmetric batteries.

Electrode	Electrolyte	Current density (mA cm^{-2})	Life (h)	Voltage polarization (mV)	Ref.
Zn-45	2 M $ZnSO_4$	0.5	3300	77.8	This work
		1.0	1680	123.3	
		2.0	1000	146.3	
DCP-Zn	2 M $ZnSO_4$	0.5	1400	60	2
$CaCO_3$@Zn	3 M $ZnSO_4$ + 0.1 M $MnSO_4$	0.25	800	105	3
PCu@Zn	2 M $ZnSO_4$	10	200	80	4
Zn@ZIF8	2 M $ZnSO_4$	0.5	680	100	5
ZnO:S@Zn	2 M $ZnSO_4$	0.5	1700	45	6
Sc_2O_3@Zn	2 M $ZnSO_4$ + 0.1 M $MnSO_4$	1.0	200	80	7
Faceted TiO_2	1 M $ZnSO_4$	1.0	460	50	8
ZnLiMn	2 M $ZnSO_4$	1.0	1000	30	9
ZnSe@Zn	2 M $ZnSO_4$	1.0	1531	32	10
$AgZn_3$	2 M $ZnSO_4$	0.25	1700	59	11
Zn/Sn@Cu foam	1 M $ZnSO_4$	1.0	1800	90	12
NiCo-LDH	2 M $ZnSO_4$	1.0	2500	20	13
NA-Zn	3 M $ZnSO_4$	0.25	2000	200	14
MoS_2@Zn	1 M $ZnSO_4$ + 1 M $MnSO_4$	2.5	180	120	15
NFZP@Zn	1 M $ZnSO_4$	2.0	900	45	16

Reference

1. T. Wang, J. Jin, X. Zhao, X. Qu, L. Jiao and Y. Liu, *Angew. Chem., Int. Ed.*, 2024, **63**, e202412057.
2. W. Guo, Z. Cong, Z. Guo, C. Chang, X. Liang, Y. Liu, W. Hu and X. Pu, *Energy Storage Mater.*, 2020, **30**, 104-112.
3. L. Kang, M. Cui, F. Jiang, Y. Gao, H. Luo, J. Liu, W. Liang and C. Zhi, *Adv. Energy Mater.*, 2018, **8**, 1801090.
4. J. Zhou, F. Wu, Y. Mei, Y. Hao, L. Li, M. Xie and R. Chen, *Adv. Mater.*, 2022, **34**, 2200782.
5. M. Cui, B. Yan, F. Mo, X. Wang, Y. Huang, J. Fan, C. Zhi and H. Li, *Chem. Eng. J.*, 2022, **434**, 134688.
6. D. L. Zhu, Y. F. Zheng, Y. Xiong, C. J. Cui, F. Z. Ren and Y. Liu, *J. Alloys Compd.*, 2022, **918**, 165486.
7. M. Zhou, S. Guo, G. Fang, H. Sun, X. Cao, J. Zhou, A. Pan and S. Liang, *J. Energy Chem.*, 2021, **55**, 549-556.
8. Q. Zhang, J. Y. Luan, X. B. Huang, Q. Wang, D. Sun, Y. G. Tang, X. B. Ji and H. Y. Wang, *Nat. Commun.*, 2020, **11**, 3961.
9. Y. Zhang, X. Yang, Y. Hu, K. Hu, X. Lin, X. Liu, K. M. Reddy, G. Xie and H. J. Qiu, *Small*, 2022, **18**, 2200787.
10. X. Yang, C. Li, Z. Sun, S. Yang, Z. Shi, R. Huang, B. Liu, S. Li, Y. Wu, M. Wang, Y. Su, S. Dou and J. Sun, *Adv. Mater.*, 2021, **33**, 2105951.
11. Y. Wang, Y. Chen, W. Liu, X. Ni, P. Qing, Q. Zhao, W. Wei, X. Ji, J. Ma and L. Chen, *J. Mater. Chem. A*, 2021, **9**, 8452-8461.
12. B. Tang, H. F. Fan, Q. F. Liu, Q. Zhang, M. Liu and E. D. Wang, *Int. J. Energy Res.*, 2022, **46**, 18562-18572.
13. C. Ma, X. Wang, W. Lu, C. Wang, H. Yue, G. Sun, D. Zhang and F. Du, *Chem. Eng. J.*, 2022, **429**, 132576.
14. M. Cui, Y. Xiao, L. Kang, W. Du, Y. Gao, X. Sun, Y. Zhou, X. Li, H. Li, F. Jiang and C. Zhi, *ACS Appl. Energy Mater.*, 2019, **2**, 6490-6496.
15. S. Bhoyate, S. Mhin, J. E. Jeon, K. Park, J. Kim and W. Choi, *ACS Appl. Mater.*

Interfaces, 2020, **12**, 27249-27257.

16. S. Wang, Z. Yang, B. Chen, H. Zhou, S. Wan, L. Hu, M. Qiu, L. Qie and Y. Yu, *Energy Storage Mater.*, 2022, **47**, 491-499.